IEEE Open Journal of
Antennas and Propagation

Received 3 July 2023; revised 20 August 2023; accepted 25 August 2023. Date of publication 1 September 2023; date of current version 22 September 2023.

Digital Object Identifier 10.1109/OJAP.2023.3311042

Low-Cost Hybrid Implementation of an Efficient E-Band Array Based on Stepped and Ridged Slots

SHERIF R. ZAHRAN [1] (Member, IEEE), EMILIO ARNIERI [1] (Member, IEEE), STEFANO MOSCATO [2], MATTEO OLDONI [3] (Member, IEEE), DARIO TRESOLDI [2], GIANDOMENICO AMENDOLA [1] (Senior Member, IEEE), AND LUIGI BOCCIA [1] (Senior Member, IEEE)

[1]MAIC-Lab, Department of Computer Engineering, Modeling, Electronics and Systems, University of Calabria, 87036 Arcavacata, Italy

[2]Research and Development Laboratories, SIAE Microelettronica, 20093 Milan, Italy

[3]Electronics, Information and Bioengineering Department, Politecnico di Milano, 20133 Milan, Italy

CORRESPONDING AUTHOR: S. R. ZAHRAN (e-mail: sherif.zahran.1991@ieee.org)

This work was supported by the Italian National Operational Program for Research and Innovation 2014–2020 through European Social Fund, Action I.1. under Grant CCI 2014IT16M2OP005.

ABSTRACT In this work, an 8×8 waveguide antenna array composed of stepped and slotted radiators for E-band applications is presented. The proposed array architecture, including the feeding network, can be realized through the integration of a single metallic block adhered with an additional top photo-etched sheet. This approach effectively reduces manufacturing complexity, resulting in a low-cost solution that can be easily fabricated using standard market-ready technologies. Array beam-forming network's building blocks: transitions, power dividers and 2×2 slotted splitters are presented. Parasitically coupled cavities, inserted in between slotted radiators, help to improve the matching and gain of the array. Stepped profile which has been applied to both active and parasitically coupled apertures, prove to enhance antenna parameters. The overall structure fills a volume of 25×24×2 mm^3. A 23.6% fractional bandwidth was achieved in the range of 69 - 86.7 GHz. Radiation characteristics were investigated for both 2×2 splitter radiators and 8×8 antenna arrays where the obtained average gain values were 12 and 25 dBi, respectively. A four-channel prototype was fabricated and measured. The measured radiation patterns agree with the simulated patterns, with a maximum aperture efficiency of 86%.

INDEX TERMS Antenna array, backhauling communications, E-Band, slotted antenna, millimeter-wave, metallic waveguide, waveguide slot array.

I. INTRODUCTION

HIGH data rates and lower latency are key drivers for the industrial wireless telecommunications market nowadays. Next generation communication networks will largely rely on the unemployed spectrum above 40 GHz, especially in commercial E-band (70-90 GHz), W-band (90-110 GHz) and D-band (110-170 GHz). Various applications, including 5G and beyond infrastructure backhauling line-of-sight (LoS) links, satellite-to-satellite space communications, autonomous automotive radars [1]. High-gain wideband antennas are required for backhauling LoS mm-wave link applications, to overcome the high absorption of electromagnetic waves caused by the atmospheric molecules at high frequencies [2].

The progressive densification of the mobile access network in urban environments does not demand few km long LoS, with an availability of 99.995% in mid/high rain-rate regions, as typical access cells are being shrunk to a few hundreds of meters apart. Moreover, fronthauling and mid-hauling network segments are dedicated to bring very high capacity between the elements of the access network, coordinated by a central unity in the area and foster short-range transport. A promising new market has emerged, characterized by links

carrying 10 Gbps/channel/polarization over distances of approximately 200 meters.

This market is expected to be highly profitable. Assuming current transmit-power levels are maintained, a gain of 39 dBi is considered sufficient to achieve this goal. Furthermore, the upcoming introduction of high-power components at mm-waves is expected to increase the effective isotropic radiated power (EIRP) by an additional 10 dB through a transmitter [3], thereby reducing the required antenna gain. In addition, the use of significantly smaller antennas allows for separate transmitting and receiving antennas to be placed on the radio equipment case, eliminating the need for duplexers and the associated losses due to internal connections between the radio-frequency chains. As a result, the required antenna gain can be reduced to 29 dBi. It is noteworthy that the interplay of several factors, such as the imperative to curtail antenna manufacturing costs, the restricted output power of front-ends, the interconnection losses, and the compact size of the radiation aperture, have engendered the emergence of various alternative configurations featuring lower gains. For example, a communication link that conventionally mandates antennas with a gain of 29 dBi could be efficiently implemented by resorting to dual channels that incorporate antennas with 26 dBi of gain or quadruple antennas that exhibit 23 dBi of gain. Nevertheless, the requisite confluence of such exigencies with cost-efficient parameters poses a formidable complexity for antenna engineers.

Throughout the years, several design proposals have been presented in the literature based on emerging technological developments, including low temperature cofired ceramic processes (LTCC) [4], [5], [6] and printed circuit board (PCB) [7], [8], [9]. Nevertheless, the highest efficiency has been usually achieved by all-metal antennas. Among the possible configurations, waveguide slot arrays (WSA) are particularly appealing for applications in which size constraints are present and integration with the electronic front-end is desired. Since they were firstly introduced [10], WSA have emerged as one of the most extensively researched antenna topics. Multiple approaches for realizing WSA have been demonstrated through the utilization of various fabrication technologies and assembly techniques. Structural realization technologies can be classified into two main categories: additive and subtractive manufacturing. The first category includes 3D printing which allows to realize complex waveguide array structures as in [11], [12], [13]. They offer restricted tolerances (>150 μm) and surface roughness while being reliant on specific materials that necessitate lengthy curing periods. These factors, in turn, hinder operational speed and increase the overall cost of prototype production. Various subtractive manufacturing techniques are available for the production of metallic waveguide arrays. Among these techniques, computer numerical control (CNC) milling constitutes a prevalent approach owing to its economical nature and ability to attain tolerances of a moderate magnitude ($\pm$30 μm), which are constrained by the milling tool diameter, as reported in [14], [15], [16], [17], [18], [19]. In an alternative approach, diffusion bonding processes can be used to realize structures with high accuracy ($\pm$20 μm) [20], [21], [22], [23], [24]. This fabrication technique involves applying heat and pressure to multiple metal layers until they form a permanent, solid-state bond. Each layer can be preliminarily etched using different technologies including chemical or laser etching. From an industrial point of view, additive manufacturing is more used for prototype realization or when low accuracy is required whereas subtractive manufacturing remains more convenient for mass production. Despite the availability of highly advanced 5-axis milling machines, the production of a waveguide array utilizing CNC necessitates machining several metal blocks. Typically, three metal layers are required: i) to implement the feeding network; ii) to host the coupling layer (or cavity backing) and iii) to implement the radiating elements. Minimizing the number of fabrication blocks is highly desirable, as it reduces manufacturing costs and mitigates the impact of mechanical, alignment, and assembly tolerances. One common strategy to reduce the manufacturing complexity and cost is to use series-feed arrangements, which, however, leads to an inherent restriction in bandwidth [11], [25], [26]. On the other hand, several attempts were made to simplify the complexity of array architectures employing corporate networks. For example, in [18] it is reported a new corporate feeding configuration which eliminates the need for a cavity-backed layer in conventional designs, allowing for a simplified assembly of only two layers. This approach utilizes E-plane T-junctions and single-ridge waveguides which necessitates stringent manufacturing accuracies and mandates the retention of inter-element spacing greater than a wavelength.

This paper outlines a novel configuration for metallic slotted arrays, with the primary goal of introducing innovative design solutions that reduce manufacturing complexity and associated costs in the context of the mobile backhauling market. As it will be shown, the proposed configuration, preliminarily introduced in [27] for D-band applications, can be manufactured by simply gluing two metal blocks fabricated using different low-cost technologies. In the proposed approach, the feed network and the radiation cavities are integrated into the first metal block through bilateral CNC machining, while the radiating slots are implemented onto a photo-etched layer. Both components can be easily manufactured using standard CNC equipment and chemical photo-etching thus ensuring cost-effectiveness throughout the entire production process. Despite the use of only two layers, the inter-element spacing is limited to 0.82 λ_0, where λ_0 is the free space wavelength. As will be expounded, the achievement of this outcome is the product of combining several innovative design solutions, such as the incorporation of parasitic radiators into the array lattice and the utilization of stepped ridged slots, which synergistically enhance the performance of the array. In the following, Section II will discuss the array geometry,

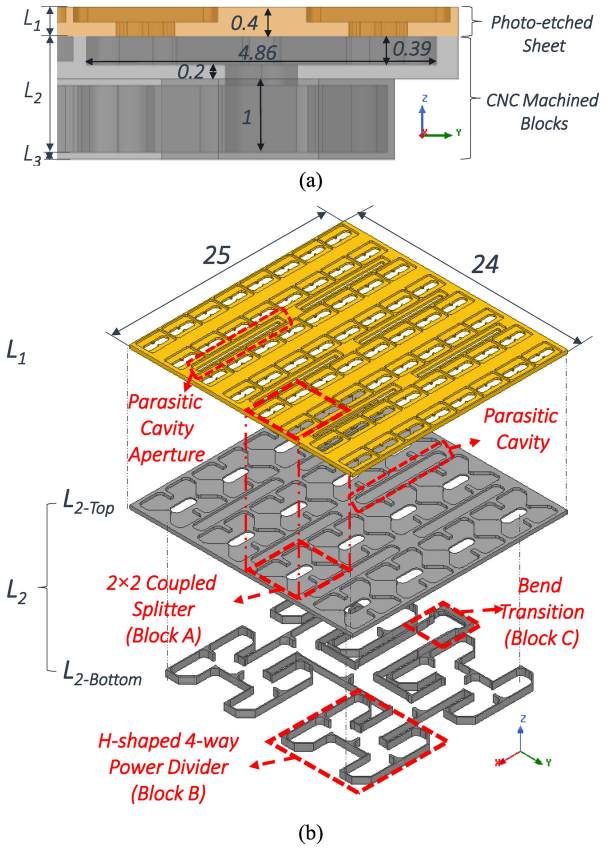

FIGURE 1. Configuration of the proposed E-band 8×8 slotted antenna array, (dimensions are in mm), (a) side view, (b) 3D sliced/exploded view.

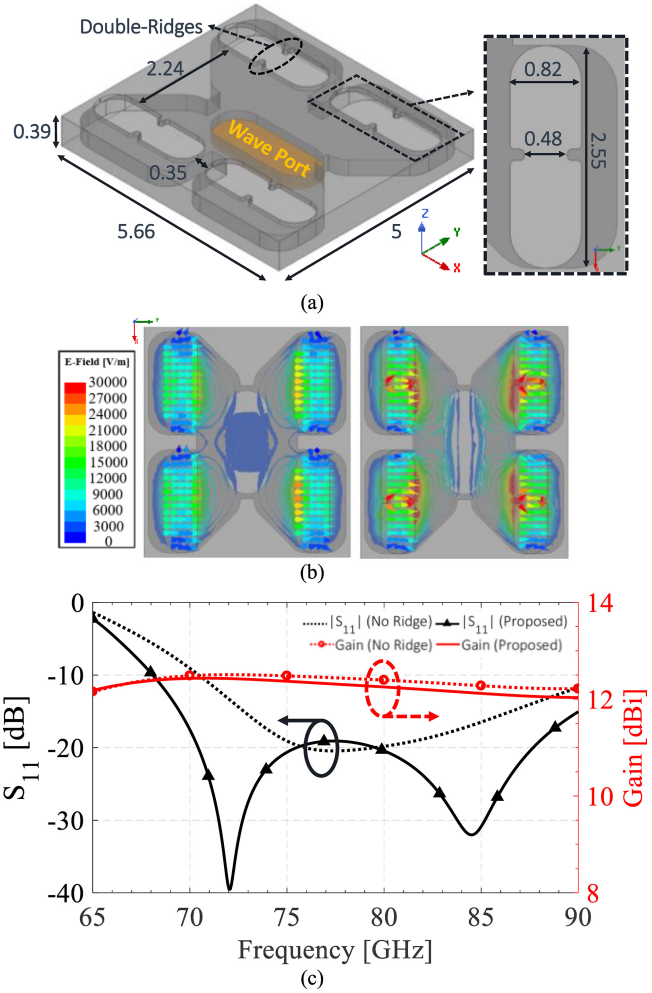

FIGURE 2. 2×2 coupled splitter *block A* (a) proposed labeled layout (dimensions in mm) (b) *E*-field distribution at 69 GHz of splitters with and without double-ridges (c) return loss and gain comparison of splitters with and without ridges.

accompanied by full-wave electromagnetic (EM) simulations of all the array building blocks. Section III will delve into the radiation performance of a 4×4 subarray, encompassing the parasitic cavities employed for performance enhancement. Furthermore, Section IV will examine the proposed 8×8 antenna array, evaluating the matching and far-field characteristics, and assessing the efficacy of the chosen gluing solution for ensuring proper electrical contact. Finally, Section V will provide a report on the measurements of the manufactured samples and compare them with the state-of-the-art.

II. ARRAY BLOCKS

Fig. 1 depicts the proposed array concept, which involves the fabrication of two metallic parts. The first part, referred to as L_1, comprises a single photo-etched sheet for implementing the slot radiators, while the second part, L_2, is CNC milled on both faces to form the corporate feeding network. A third layer, L_3, functions as a bottom cover and flange to mount the WR12 waveguide utilized for feeding the array. As illustrated in Fig. 1 (b), the antenna array is formed by the combination of the following blocks: a) *Block A*, 2×2 coupled splitter and slotted-antenna, b) *Block B*, H-shaped 4-way power divider, and c) *Block C*, WR12-to-custom-WG bend transition. *Block A* serves the purpose of providing an additional power split and hosts the radiating slot cavities. *Block B* comprises an H-plane 4-way power divider that ensures uniform signal distribution. The final antenna is fed through a standard WR12 waveguide which is then converted to a custom rectangular waveguide through an E-band transition (*Block C*). This section discusses the design of each block used to realize the final antenna array. It is worth to mention that all presented blocks are modelled using Aluminum material (3.8×10^7 Siemens/m).

A. 2×2 COUPLED SPLITTER AND ANTENNA (BLOCK A)

The basic radiating cell of the proposed array, array unit cell, is a group of four slots cut on the photo-etched metal sheet. This key block is integrated with a 2×2 (four-way) power splitter, as illustrated in Fig. 2 (a), fed vertically through a rounded waveguide aperture. This metal sheet is critical as, from its behavior depends not only the performance of the entire array but also the ability to implement the simplified manufacturing approach reported in Fig. 1. For this reason, this block fully exploits the manufacturing capabilities of the photo-etched technology by using metal slots. To facilitate the mechanical manufacturing of the array, all internal

corners are filleted with a radius of 0.45 mm so it can be machined with standard 0.4 mm radius milling tool. Four radiator slots are engraved on the top to couple the power to the desired mode and radiate a linear polarization.

Each radiating element is configured as a curved-edge slot with double-ridges, as represented in Fig. 2(a). The modelling and simulations were performed using a commercial finite element software [28]. As employed in [16], [29], the presence of ridges enhances slots' E-field intensity at lower frequencies. As shown in Fig. 2(b), where two models of the coupled splitter without (left) and with (right) double-ridges are compared at 69 GHz both with 90° phase. Fig. 2(c) is a comparison between the return loss of the 2×2 coupled splitter without and with double-ridges where a 2 GHz enhancement in operational BW can be observed when considering the lower spectrum at the required 10 dB return loss level. On the other hand, boresight gain is slightly reduced by 0.2 dB at 90 GHz, which can be acceptable considering the BW enlargement. Targeting a minimum element spacing for both E-plane and H-plane considering constrains implied by utilized technologies. From center, the spacing between radiating slots in E-plane and H-plane directions are 0.77 λ_o and 0.86 λ_o, respectively, therefore no grating lobes are expected in the far-field radiation pattern. It is worth to mention that such radiating slots, considering the double-ridges, are impossible to be realized using current commercial CNC machining technology.

B. H-SHAPED 4-WAY POWER DIVIDER (BLOCK B)

The bottom-side of L_2 hosts the second level of the array distribution network which consists of four H-shaped 4-way power dividers. The proposed H-shaped power divider, *Block B,* is composed of dual T-junctions used to split the signal into 4 ways with equal magnitude and phase while converting each port waveguide from horizontal to vertical to feed each 2×2 coupled splitter radiator. The T-junctions were designed following the approach proposed in [27], [30]. The design of the power divider was carried out as a tradeoff between the desired operational BW of the whole corporate feeding network and the array element-spacing, which must be compatible with acceptable grating lobe levels (GLL). Thus, for achieving array structural-uniformity, the cross-section of the WG used to feed the power divider is reduced from WR12 standard size to be with size of 2.25×1 mm^2. With such width, the useful BW starts from 73.5 GHz since the cut-off frequency is shifted upwards by 10 GHz. It is important to mention that this choice has been taken to privilege element's pitch over waveguide dispersion and losses.

The 3D view of the proposed power divider with labeled dimensions is shown in Fig. 3(a), where the overall size of the power divider is 8.4×9.4 mm^2. Fig. 3(b), illustrates the simulated S-parameters response of the designed power divider. It can be observed that the insertion loss level is the same for all four ports averaged at 0.8 dB while the return loss is better than 12 dB from 71 to beyond 86 GHz.

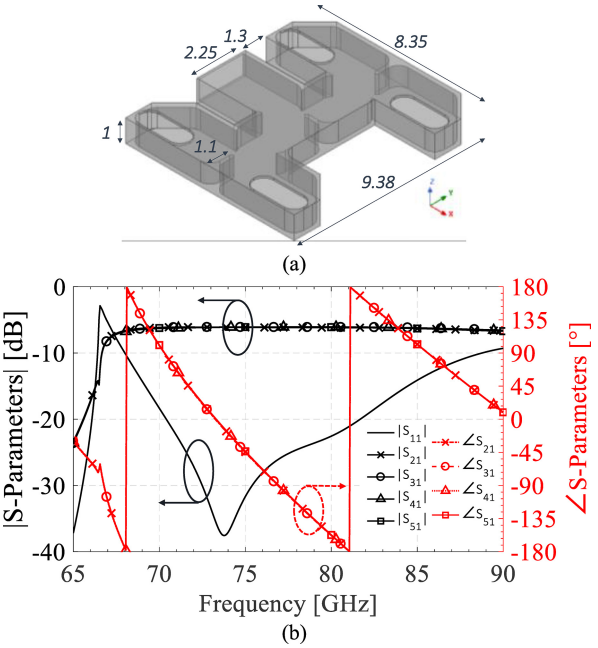

FIGURE 3. H-shaped power divider Block b (a) simulation model (dimensions in mm) (b) S-parameters.

Thanks to the structure symmetry, equal phase is observed at all four ports.

C. WR12-TO-CUSTOM-WG BEND TRANSITION (BLOCK C)

The most effective way to avoid extra routing between the power divider and the radiator is to place the antenna directly on top of a sealed in-package transition as proposed in [31], imposing that the antenna should be fed vertically as in [27]. Additionally, the main corporate-feed network is composed of many H-shaped four-way power dividers inter-connected with a reduced size waveguide (2.25×1 mm^2) as labeled in Fig. 4(a). Therefore, a need arises for a structure that transforms this horizontal reduced/size waveguide to a vertical one sized as a standard WR12 (3.1×1.54 mm^2). It is important to mention that the inner corners of such structure must be compatible with the radius of the milling tool which will be used for realization. Fig. 4(a), show the transparent 3D view of the proposed transition. Fig. 4(b) represents the simulated transmission and reflection coefficients of this transition: the return loss is better than 20 dB starting from 71 till more than 86 GHz, while the insertion loss is lower than 0.1 dB across the operational bandwidth.

III. 4×4 ANTENNA SUBARRAY AND PARASITIC SLOTTED CAVITIES

A subarray can be constructed by combining one H-shaped power divider to four 2×2 coupled slotted splitters as depicted in Fig. 5(a). Although the spacing of each sub-block is minimal, the size of the H-shaped power dividers enforces a distance between the radiating slots exceeding 2.24 mm along the E-plane, which corresponds to a center-of-phase spacing approaching the wavelength at the highest operating

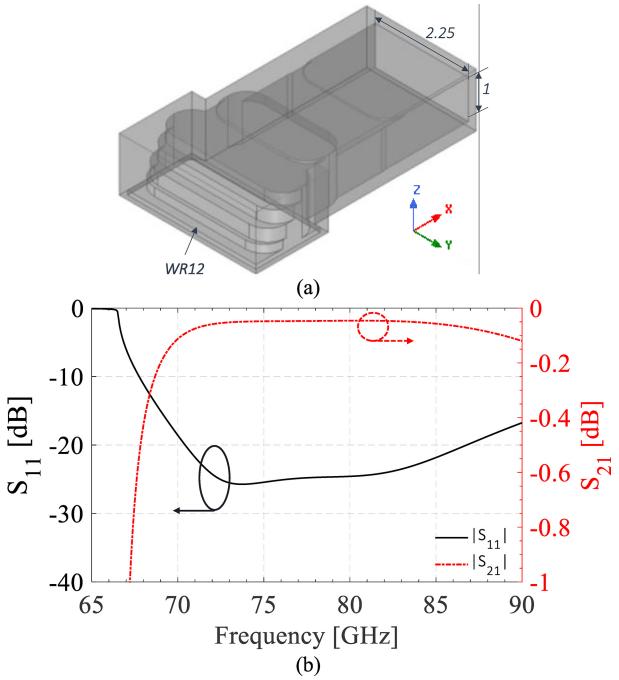

FIGURE 4. Designed WR12 to custom WG E-bend transition, (dimensions are in mm), (a) 3D view (b) S-parameters versus frequency response.

frequency. An important aspect worth considering is that any further reduction in the spacing between radiating slots would necessitate the addition of an extra layer in the antenna build-up, a measure that is incompatible with the design principle aimed at simplifying the manufacturing and assembly process. Therefore, this limitation poses a significant challenge to the design of the H-shaped power divider-based antenna. To overcome this challenge, one of the key novelties of this work is the incorporation of a passive slotted cavity along the H-plane between each pair of neighboring 2×2 splitters, as illustrated in Fig. 5(b). These cavities are parasitically coupled to the radiating elements via metallic slots and effectively mitigate mutual coupling by suppressing surface waves. As a result, the performance of the antenna is significantly enhanced without compromising its manufacturing and assembly simplicity. Previous research, as reported in [7], presented a similar approach whereby metallic grooves with a depth of one-quarter wavelength were utilized to control lateral waves and array coupling. However, in contrast to this previous configuration, the present work adopts cavities as a means of controlling the interaction between adjacent elements. By manipulating the active impedance, the use of such cavities can enhance the array gain, avoid grating lobes, and offer additional flexibility in the antenna design. Proposed cavities have a rounded shape of length 9.7 mm and width 1.22 mm while the parasitic radiating aperture has length of 9.3 mm and width of 0.4 mm. Cavities can be embedded into the top metal block and, for the application at hand, are used to improve the array matching and harmonize the radiation pattern by increasing the antenna gain as will be shown next.

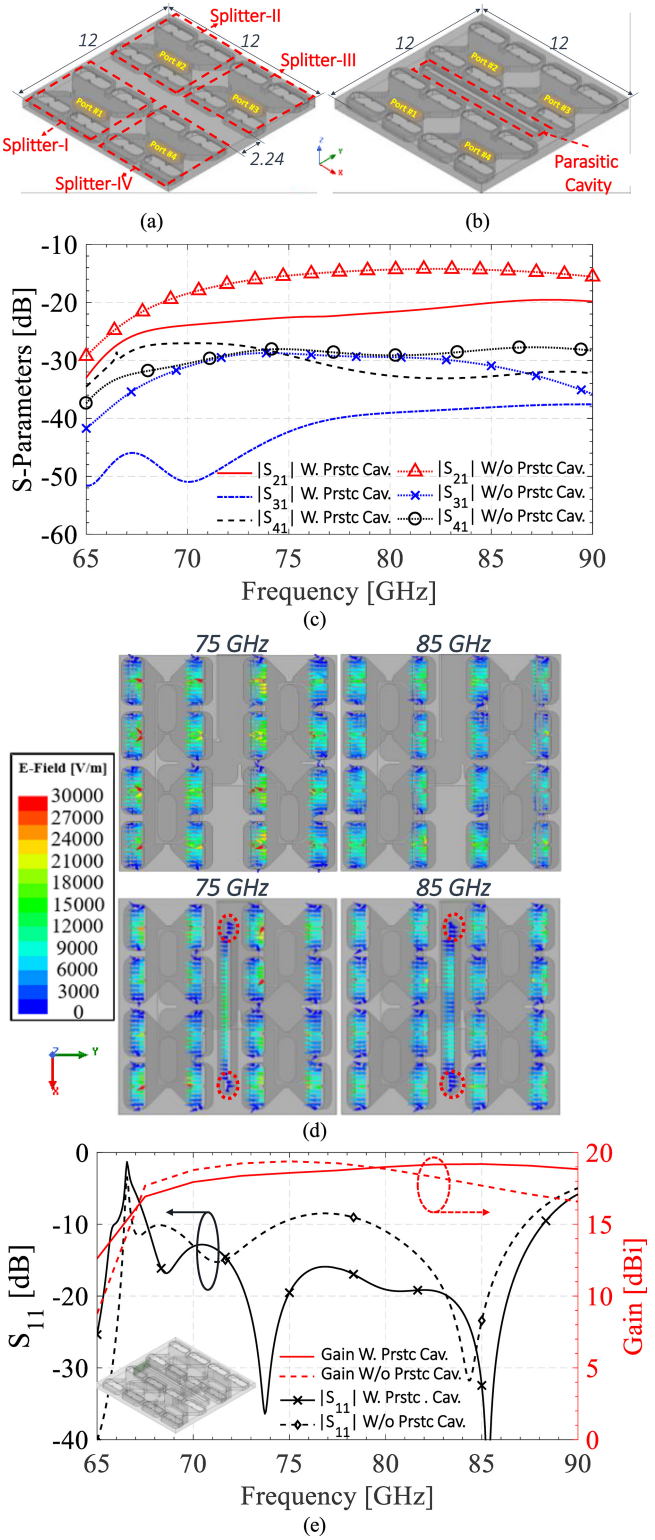

FIGURE 5. (a) 4×4 antenna subarray (b) 4×4 subarray with added parasitic cavity (dimensions in mm) (c) mutual coupling between fed 2×2 splitters (d) Electric field distribution at all slots (e) return loss and gain comparison of subarrays + H-shaped power divider without and with parasitic cavity.

To calculate mutual coupling, all four splitters, *Block A*, were excited using wave-ports without and with the presence of the proposed cavity. Fig. 5(c) shows the comparison

of the mutual coupling between ports with and without parasitic cavity. It is observed that mutual coupling between Splitter-I and Splitter-II, denoted as $|S_{21}|$, is reduced from -14.5 dB to -22 dB at f_0. While mutual coupling between Splitter-I and Splitter-III, $|S_{31}|$, is reduced from -29.4 dB to -39.5 dB. Concerning the mutual coupling between Splitter-I and Splitter-IV, $|S_{41}|$, it remains about -32 dB for both scenarios yet, it is less sensitive across the observed BW if the passive cavity is considered.

Two models were simulated, both combine between a single H-shaped power divider and proposed 4×4 subarray, without and with parasitic cavity. To further understand the effect of the parasitic cavity, the electric field distribution, as seen from all slots is plotted at different frequencies for both simulation scenarios as presented in Fig. 5 (d). Passively reflected radiation from the parasitic cavity, due to its superposition, is the resultant of the interference of surface waves at a given frequency as shown in Fig. 5 (d). The induced electric field in the parasitic cavity is coherent with the one excited from all radiating slots especially in middle region. The existence of such cavity affects the reflection coefficient and the gain of the antenna drastically as indicated in Fig. 5(e).

With the presence of the parasitic cavity, the reflection coefficient is improved from -8.5 dB at 77 GHz to -16 dB, while the boresight gain is reduced from 19.25 dBi to 18.75 dBi at 77.5 GHz. This is due to the misalignment/shift in E-field of reflected waves along H-plane, as observed from the parasitic cavity, with respect to the E-field from all 4×4 subarray slots. An opposite scenario is noticed at higher frequencies, after 80 GHz, where the gain is much improved when the passive cavity is present: for example, at 87.5 GHz the gain is increased from 17.1 dBi to 19.1 dBi.

The final geometrical dimensions of the added slotted parasitic cavity are achieved thanks to parametrical analyses. These studies consider the main design dimensions eligible for practical realization. It is important to mention that such dimensions are bounded by the surrounding structures and realization technology restrictions, e.g., the width of the cavity is limited by the radius of the used milling tool and the side walls of the 2×2 splitters, including the prober margin needed for structural robustness, so this dimension is bounded by 0.8-1 mm and thus not included in the parametric study. Three dimensions are investigated to reach the final design, these dimensions are the length of cavity (L_{RC}), the depth of cavity (H_{RC}), and the width of the cavity slot aperture (W_{RCSlot}), as labelled in the subfigures of Fig. 6 (a), (b) and (c), respectively.

As shown in Fig. 6 (a), the longer the cavity the lower the mutual coupling and thus the better the matching, when compared with a design without a cavity. Yet, if the length is small, bad boresight gain can result due to surface waves interference as explained previously, especially, at higher frequencies. Similarly, better matching is observed when the depth of the cavity is increased as depicted in Fig. 6 (b). However, the milling tool is bounded and can't go deeper

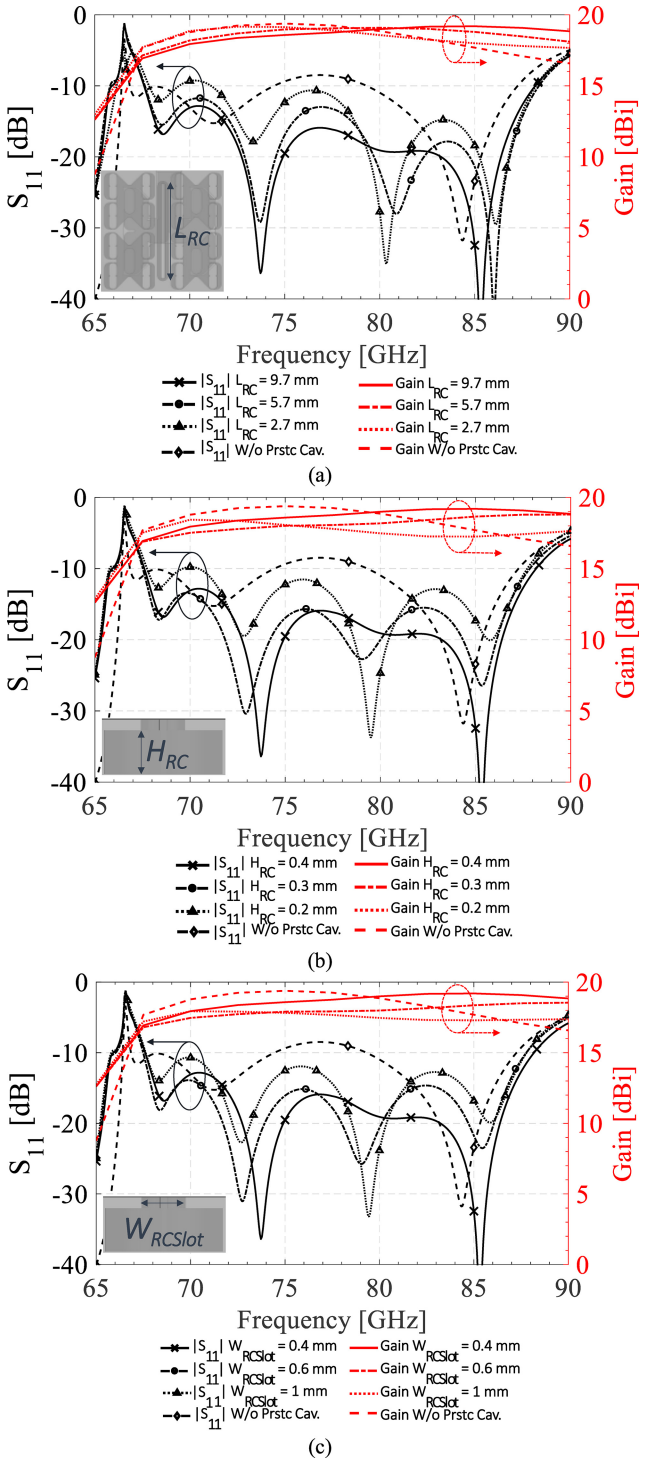

FIGURE 6. Parasitic cavity parametric analysis of the proposed 4×4 subarray (a) length of cavity (b) cavity depth (c) cavity aperture slot width.

without penetrating the lower layer ($L_{2-Bottom}$). Gain at high frequencies is directly proportional to the depth of the cavity.

The width of the top cavity slot can be an added degree of freedom as the photo-etching technology allows the realization of narrower engravings. From Fig. 6(c), the narrower the top cavity slot becomes, better matching is obtained, and the gain values are increased across the observed BW.

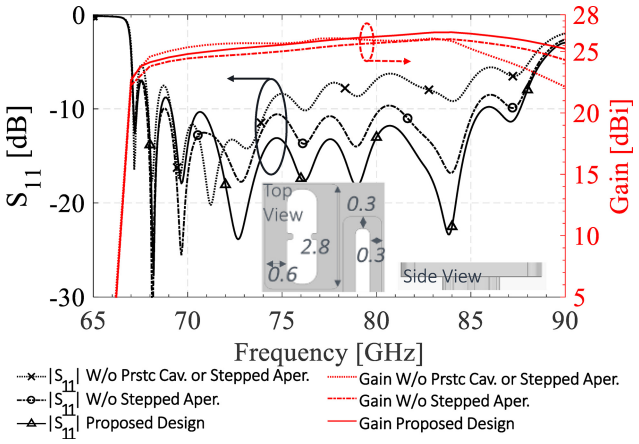

FIGURE 7. Simulated return loss and boresight gain comparison of 8×8 arrays without parasitic cavities/stepped apertures, without stepped apertures and proposed array (subfigure: cut-down stepped apertures dimensions in mm).

IV. 8X8 ARRAY DESIGN AND INTEGRATION

A. ARRAY DESIGN AND OPERATION

Building upon the promising results of the 4×4 subarray, a full uniform 8×8 array has been designed. The three-dimensional exploded view of the proposed 8×8 antenna array is presented in Fig. 1 (b), showing the first two layers. Where L_2 is designed to be CNC machined from both sides from a single block of metal. The circuit included in the bottom part of L_2, referred to as $L_{2\text{-}Bottom}$, comprises four connected power dividers and a single WR12-to-custom-WG bend transition. The blocks machined on the top part of L_2, referred to as $L_{2\text{-}Top}$, include 16 coupled splitters. The 64 radiating slots are implemented through photo etching technique on a 0.4 mm thick aluminum sheet L_1 with total size of 25×24 mm^2.

The antenna operates in transmission as follows. An input signal is fed through a WR12 waveguide and it is then translated and bent by 90° into a custom-sized waveguide using the designed bend transition. The signal is then horizontally fed to a corporate beam forming network (BFN) consisting of 4 H-shaped 4-way power dividers. These power dividers divide the signal and then couple them vertically to feed an array of 2×2 coupled splitters, each with four ridged-slot radiators and passive air cavities in between, as described in Section III.

The complete array, including all layers, was modeled and simulated. The simulated reflection coefficient and gain are reported in Fig. 7. This figure includes the results of the array with and without parasitic cavities. As it can be observed, such cavities improve matching, gain and radiation properties. However, especially in the upper portion of the band, these parameters degrade with a significant gain drop beyond 85 GHz.

The slotted apertures, in L_1, were cut-down to have a stepped profile which can be an additional corrugation to further suppress surface waves and thus enhance the overall array response. This stepped profile can be easily fabricated

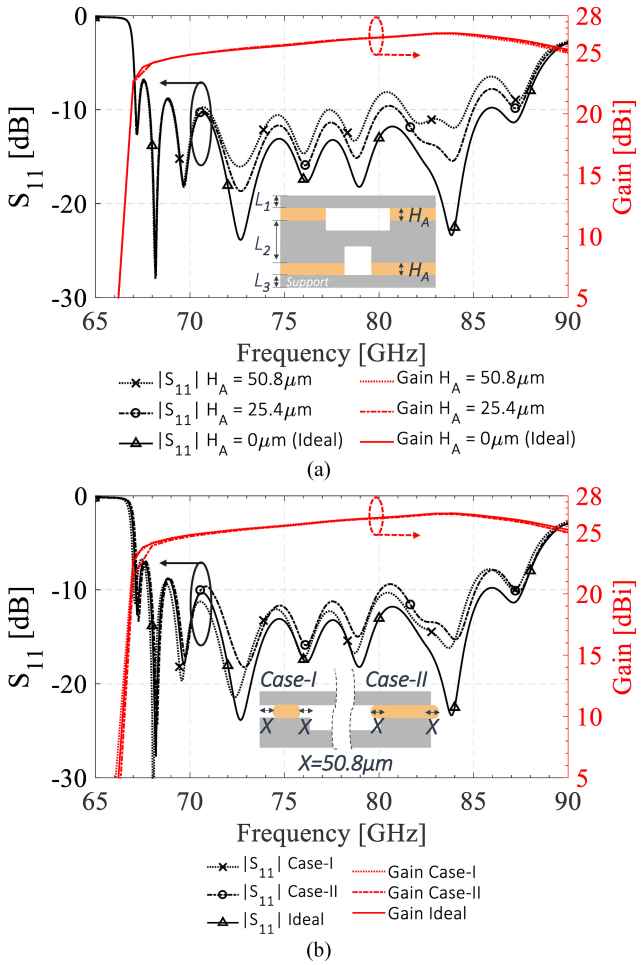

FIGURE 8. Array assembly sensitivity study (a) adhesive thickness tolerance (b) adhesive contraction/shrinkage.

as chemical photo etching technology offers the possibility to fabricate a ≈50% cut-down, from sheet thickness. Stepped profile has been implemented for both active and parasitic slotted apertures with shown dimensions in the subfigure of Fig. 7. As reported in Fig. 7, an overall improvement in both return loss and gain can be noticed at the middle of the spectrum, $S_{11} \geq 2$ dB and gain ≈ 0.5 dBi are better thanks to the stepped profile of the slotted radiators. The overall S_{11} of the proposed design exhibits more than 10dB from 69GHz to 87GHz with a gain ranging from 24dBi to 26dBi.

B. ARRAY ASSEMBLY SENSITIVITY STUDY

The proposed array layers are designed to be attached together using Loctite ABLESTIK 3350CF conductive adhesive, which is available in solid-sheet form. The selected adhesive has thickness of 50.8 μm, volume resistivity of 4×10^{-4} Ω-cm and curing time of 30 minutes at 150°C. The aim is to laser- cut two adhesive films and place them in-between L_1-L_2 and L_2-L_3 then uniformly apply pressure and heat required for curing. Such processes are subjected to uncertainty related to final thickness of the

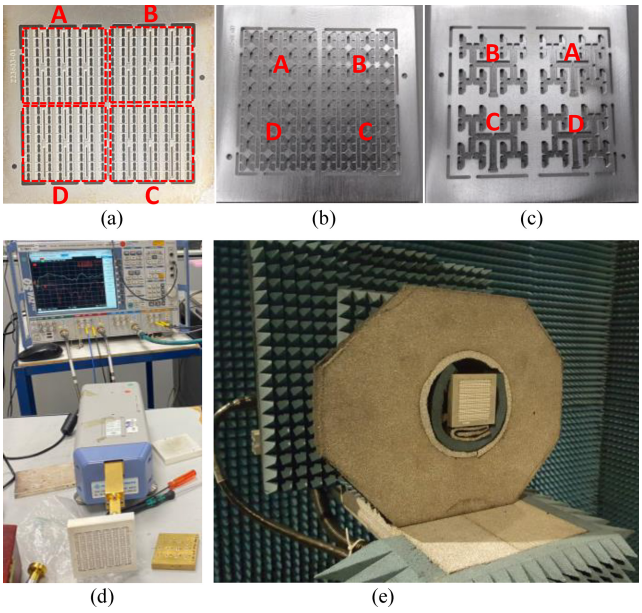

FIGURE 9. Manufactured prototype and measurement: (a) photo-etched sheet L_1 [four channels are highlighted with red dotted-frame] (b) top $L_{2\text{-}Top}$ views of the CNC milled block (c) bottom $L_{2\text{-}Bottom}$, (d) return loss measurement setup (e) far field measurement inside anechoic chamber.

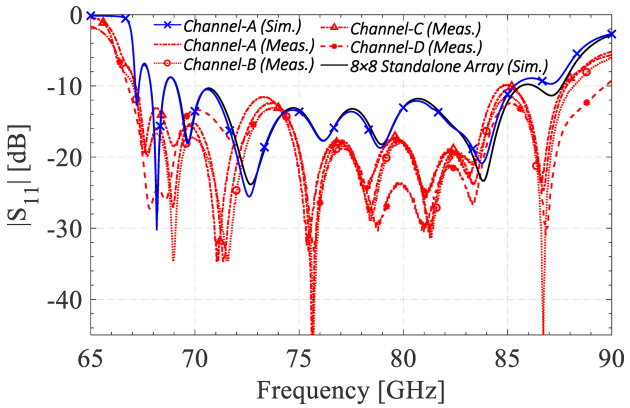

FIGURE 10. Simulated and measured reflection coefficient vs frequency.

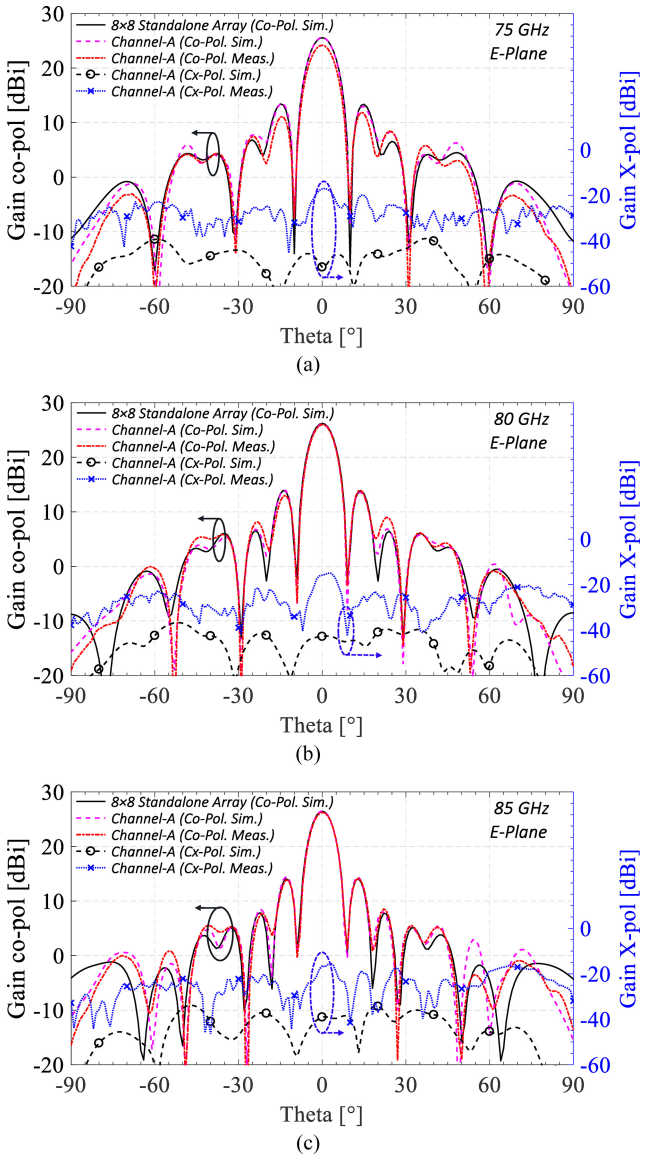

FIGURE 11. Simulation vs measurement far field radiation pattern E-plane.

adhesive after curing. Additionally, reduced/over pressure, required for curing of the adhesive, may lead to shrinkage/leakage within the waveguide cavity. In this sub-section, two studies are presented to address these assembly-related aspects.

Firstly, two layers of adhesive film with variable thickness (H_A) were added to the proposed array in-between L_1-L_2 and L_2-L_3 as illustrated in the subfigure of Fig. 8 (a). The proposed array has been simulated three times where H_A has been assigned with values of 0 (Ideal), 25.4 and 50.8 μm. As shown in Fig. 8 (a), more degradation is noticed in the reflection coefficient as H_A increases with rate of 1 dB at center frequency. The gain values are negligibly affected by H_A variation. Secondly, two layers of adhesive film were added to the proposed array in two scenarios to represent shortage/contraction of adhesive between layers (*Case-I*) and excessiveness/leakage of adhesive inside the waveguide cavity (*Case-II*). As demonstrated in the subfigure of Fig. 8 (b), in both scenarios the rate of change (X) kept constant with value of 50.8 μm. The two deformation phenomena generate similar effects: a slight degradation of S_{11} with respect to the ideal case, reaching –8dB at 86 GHz. The gain response is instead affected by less than 0.1dB.

V. EXPERIMENTAL VALIDATION

The fabricated test vehicle is implemented by placing four such identical arrays in a 2×2 grid, aiming at increasing the data rate through multi-channel usage, with each channel ideally fed by its own RF stream. Fig. 9 (a) is a photograph of the top view of the chemically photo-etched metallic sheet (L_1). The four channels of the test vehicle are denoted by channel-A, -B -C and -D. The top and bottom views of the manufactured CNC machined block ($L_{2\text{-}Top}$ and $L_{2\text{-}Bottom}$ on

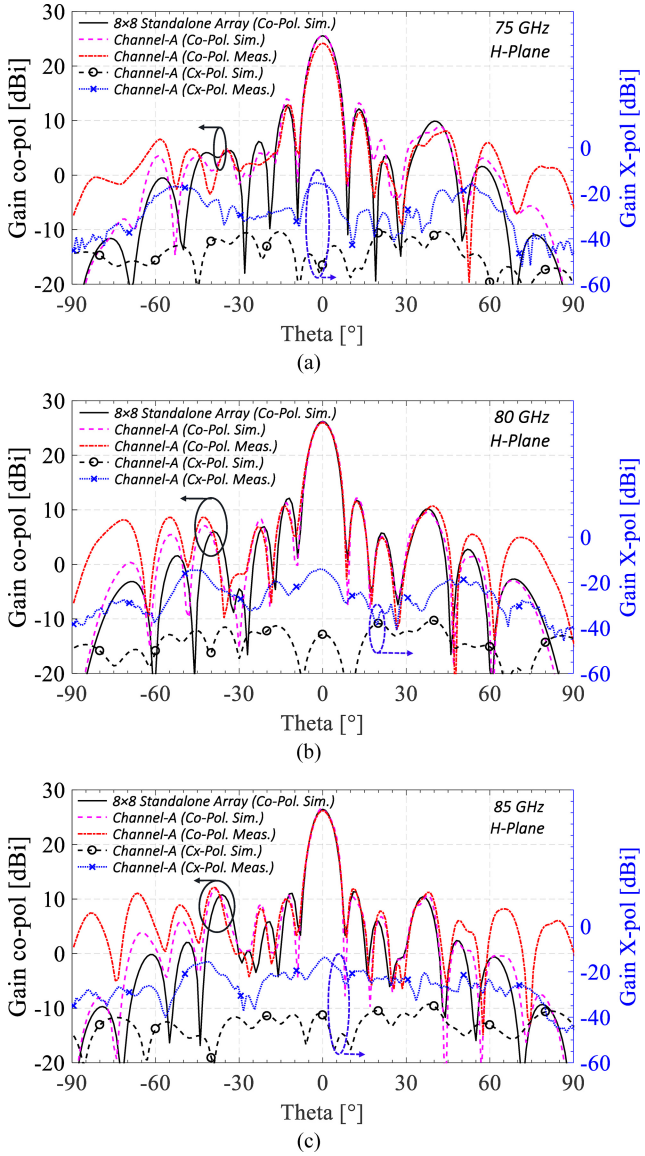

FIGURE 12. Simulation vs measurement far field radiation pattern H-plane.

either side) are shown in Fig. 9 (b) and (c), respectively. L_1 and L_2 were assembled through two alignment posts and adhered using a 50 μm-thick Loctite ABLESTIK 3350CF conductive adhesive. Return loss measurements have been carried out through a vector network analyzer (VNA) with external frequency extenders operating up to 110 GHz as shown in Fig. 9(d). Far field measurements, as shown in Fig. 9 (e), were done within 75 – 85 GHz frequency range.

In order to assess the final performance of the full test vehicle, the proposed 8×8 array has been simulated and compared in Fig. 10 with the expected standalone performance (the "Proposed" curve of Fig. 7), showing identical matching. Comparisons between simulated and measured reflection coefficients of the proposed array are presented in Fig. 10. Simulated scenarios show identical matching.

TABLE 1. Measured half-power beam width (HPBW).

	Meas. HPBW E-PLANE	Meas. HPBW H-Plane
75 GHz	8.6°	7.8°
80 GHz	8.1°	7.8°
85 GHz	7.7°	7.6°

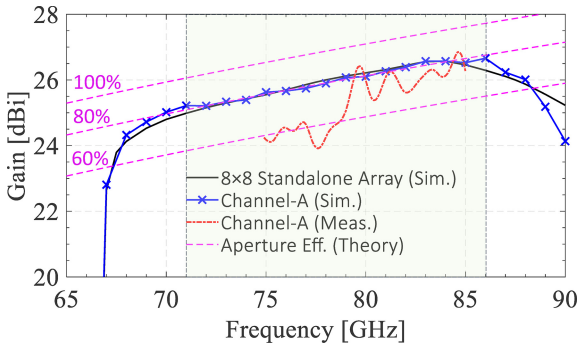

FIGURE 13. Boresight gain versus frequency of the full proposed array (dashed purple lines highlight the theoretical gain boundaries give the aperture efficiency).

A good agreement is observed between simulation and all four measured channels (-A, -B -C and -D) except for a minor shift between curves at lower frequencies which doesn't affect the antenna functionality. This shift is due to tolerances of laser-cut adhesive film additional to minor manufacturing error of the photo-etched sheet. Optical investigations showed ± 50 μm tolerance variation, especially, in the realized double ridges and inner-borders of the stepped profile between realized slots. Yet, the achieved 10-dB RL fractional bandwidth is 23.6%, from 67.1 to 87.8 GHz covering whole E-band. The radiation characteristics of the array were first investigated by considering the far field radiation patterns at 75, 80 and 85 GHz on the E- and H-planes, as shown in Fig. 11 and 12, respectively. The E-plane comparison shows a perfect agreement between simulation and measured patterns at all frequencies. The difference between co- and cross-polarization remains over 40 dB in the broadside direction. On the other hand, Fig. 12, indicates that H-plane pattern simulation and measurements, of Channel-A, are identical. It is worth mentioning that discrepancy is noticed between simulated standalone 8×8 array and channel-A especially in H-plane. This is due to mutual coupling between the horizontal channel pairs (e.g., Channel-A and Channel-B) as discussed previously in Section III. Yet, this does not alter the main functionality of the antenna array.

The half-power beam width (HPBW) is bounded between −8.6° and 7.8° for both E and H-planes for all measured frequencies, as listed in Table 1. A comparison between simulated and measured boresight gain against frequency for the proposed 8×8 antenna array is illustrated in Fig. 13. A slight minor difference between gain values for both cases is noticed after 75 GHz which can be a result of manufacturing imperfections. Oscillations in the measured gain curve are attributed to Coaxial W1-to-WR10 adapter that was employed to feed the, WR12 fed, antenna. Yet, at the upper

TABLE 2. Metallic antenna arrays state-of-the-art.

Year Ref.	Technology	Scale / No. of Fab. Layers	Return Loss (< 10 dB) [GHz]	f_o [GHz]	10dB FBW	Element Spacing /λ_o	Aperture Size (λ_o^2)	Max. Gain	Aperture Efficiency
2019 [12]	3D Printed	16×16 / 4	28.2-35.8	31	23.8%	0.95	15.14 × 15.14	33.8	85.0%
2016 [14]	CNC Milling	8×8 / 4	10.24–14.87	12	36.9%	0.89	7.3 × 7.3	26.3	60.0%
2018 [15]	CNC Milling	32×32 / 3	71-86	78.5	20.0%	0.82	26.3 × 26.3	38	70.0%
2019 [16]	CNC Milling	8×8 / 2	56.5-67	62	17.0%	0.86	6.89 × 6.89	26	70.0%
2019 [17]	CNC Milling	8×8 / 3	28.3-35.3	31	22.6%	0.78	6.25 × 6.25	23.5	85.0%
2021 [18]	CNC Milling	32×32 / 3	71-86	78.5	19.0%	1.08	31.28 × 31.28	40	82%
2018 [20]	Diffusion Bonding	16×16 / 24	120-160	140	15.1%	1.06	16.53 × 16.53	31.7	83.0%
2014 [21]	Diffusion Bonding	32×32 / 12	119-134	125	16.0%	1.72	27.23 × 27.23	38	60.0%
		64×64 / 12	118.5–133	125	11.6%	1.72	56.48 × 56.48	43	50.0%
2011 [22]	Diffusion Bonding	16×16 / 11	58.8-63.9	60	8.3%	0.87	13.89 × 13.89	33	83.6%
2012 [24]	Diffusion Bonding	16×16 / NA	60-65	62.5	8%	0.85	15.8 × 15.6	33	>70%
This work	CNC Milling & Photo-etching	8×8 / 2*	69-86.7	78.5	23.6%	0.86	6.16 × 6.56	26.4	86.2%

* Using the transition proposed in [31]. The required antenna block for fabrication are only 2 as the bottom layer will be the replaced by the package cover.

critical frequencies, curves remain in line with simulation. The highest boresight gain value is 26.4 dBi at 79.7 GHz. Given the aperture area of 23.2 × 24.68 mm^2, the aperture efficiency can reach up to 86.2%.

A comparison between the proposed design with state-of-the-art publications, is presented in Table 2. Similar work based on CNC machining and with reduced number of layers targeting *E*-band are reported in [15] and [18] can be considered as fair opponents. Yet, both [15] and [18], have reduced performance in terms of FBW and reported measured aperture efficiency. With respect to other configurations reported in Table 2, the proposed design is inspired by an extreme simplification of the manufacturing process to adhere to the industrial requirements for low-cost fabrication. Nevertheless, the use of parasitic cavities and stepped slot apertures assured a clear advantage in terms of FBW and aperture efficiency with respect to the state-of-the-art.

VI. CONCLUSION

In this work, a broadband E-Band antenna array based on corporate-fed slotted radiators has been considered. The proposed solution is suitable for low-cost millimeter-wave backhauling industrial applications. The antenna array could be machined easily from a single metallic block and a single photo-etched sheet. With the aid of parasitically coupled dummy cavities and stepped-slot apertures, a significant improvement in the overall matching and gain has been reported. The proposed 8×8 array achieves a measured FBW of 23.6% from 67.1 to 87.8 GHz covering the E-band spectrum. Measured far field radiation characteristics are in line with the simulated ones where at 79.7 GHz the boresight gain is 26.4 dBi and the aperture efficiency is 86.2%. The proposed uniform structure can be easily scaled to obtain larger, more directive arrays by machining a larger corporate feeding network.

ACKNOWLEDGMENT

The Authors wish to thank C. Franceschet, Ph.D., with the Physics Department of the Università degli Studi di Milano, Milan, Italy, for the measurement of the antenna patterns in anechoic chamber. The Authors also extend their gratitude to A. Manuzzi with SIAE's Clean Rooms Dept. for his valuable help in assembling the manufactured antenna samples.

REFERENCES

[1] T. S. Rappaport et al., "Millimeter wave mobile communications for 5G cellular: It will work!," *IEEE Access*, vol. 1, pp. 335–349, 2013, doi: 10.1109/ACCESS.2013.2260813.

[2] L. Luini, G. Roveda, M. Zaffaroni, M. Costa, and C. Riva, "EM wave propagation experiment at e band and d band for 5G wireless systems: Preliminary results," in *Proc. 12th Eur. Conf. Antennas Propag. (EuCAP 2018)*, London, U.K.: Institution of Engineering and Technology, 2018, pp. 1–5. doi: 10.1049/cp.2018.0378.

[3] M. Oldoni, S. Moscato, G. Biscevic, G. L. Solazzi, and G. Skiadas, "A mmWave power booster for long-reach 5G wireless transport," *Microw. J.*, vol. 22, no. 9, pp. 90–96, Sep. 2022. [Online]. Available: https://www.microwavejournal.com/articles/38820-a-mmwave-power-booster-for-long-reach-5g-wireless-transport

[4] A. C. Bunea, D. Neculoiu, M. Lahti, and T. Vaha-Heikkila, "Substrate integrated waveguide fed LTCC microstrip patch antenna for 94 GHz applications," in *Proc. 2015 Int. Semicond. Conf. (CAS)*, Sinaia, Romania, Oct. 2015, pp. 127–130, doi: 10.1109/SMICND.2015.7355184.

[5] F. Sickinger, E. Weissbrodt, and M. Vossiek, "76–81 GHz LTCC antenna for an automotive miniature radar frontend," *Int. J. Microw. Wirel. Technol.*, vol. 10, nos. 5–6, pp. 729–736, Jun. 2018, doi: 10.1017/S1759078718000855.

[6] B. Zhang et al., "Integration of a 140 GHz packaged LTCC grid array antenna with an InP detector," *IEEE Trans. Compon. Packag. Manuf. Technol.*, vol. 5, no. 8, pp. 1060–1068, Aug. 2015, doi: 10.1109/TCPMT.2015.2453407.

[7] K. Fan, Z.-C. Hao, Q. Yuan, G. Q. Luo, and W. Hong, "A wideband high-gain planar integrated antenna array for *E*-band backhaul applications," *IEEE Trans. Antennas Propagat.*, vol. 68, no. 3, pp. 2138–2147, Mar. 2020, doi: 10.1109/TAP.2019.2948492.

[8] H. Arakawa, H. Irie, T. Tomura, and J. Hirokawa, "Suppression of E-plane sidelobes using a double slit layer in a corporate-feed waveguide slot array antenna consisting of 2 × 2-element radiating units," *IEEE Trans. Antennas Propagat.*, vol. 67, no. 6, pp. 3743–3751, Jun. 2019, doi: 10.1109/TAP.2019.2902677.

[9] S. M. Sifat, M. M. M. Ali, S. I. Shams, and A.-R. Sebak, "High gain bow-tie slot antenna array loaded with grooves based on printed ridge gap waveguide technology," *IEEE Access*, vol. 7, pp. 36177–36185, 2019, doi: 10.1109/ACCESS.2019.2902596.

[10] L. V. E. Williams, "The physical principles of wave guide transmission and antenna systems." W. H. Watson. Oxford, U.K.: Clarendon Press, 1947, pp. xiii + 208. (Illustrated.) $7.00, *Science*, vol. 106, no. 2763, pp. 601–601, 1947.

[11] G. P. Le Sage, "3D Printed waveguide slot array antennas," *IEEE Access*, vol. 4, pp. 1258–1265, 2016, doi: 10.1109/ACCESS.2016.2544278.
[12] Y. Li et al., "3-D printed high-gain wideband waveguide fed horn antenna arrays for millimeter-wave applications," *IEEE Trans. Antennas Propagat.*, vol. 67, no. 5, pp. 2868–2877, May 2019, doi: 10.1109/TAP.2019.2899008.
[13] J. Tak, A. Kantemur, Y. Sharma, and H. Xin, "A 3-D-printed W-band slotted waveguide array antenna optimized using machine learning," *Antennas Wirel. Propag. Lett.*, vol. 17, no. 11, pp. 2008–2012, Nov. 2018, doi: 10.1109/LAWP.2018.2857807.
[14] Z. Shi-Gang, H. Guan-Long, P. Zhao-hang, and L.-J. Ying, "A wideband full-corporate-feed waveguide slot planar array," *IEEE Trans. Antennas Propagat.*, vol. 64, no. 5, pp. 1974–1978, May 2016, doi: 10.1109/TAP.2016.2526074.
[15] P. Liu, J. Liu, W. Hu, and X. Chen, "Hollow waveguide 32 × 32-slot array antenna covering 71–86 GHz band by the technology of a polyetherimide fabrication," *Antennas Wirel. Propag. Lett.*, vol. 17, no. 9, pp. 1635–1638, Sep. 2018, doi: 10.1109/LAWP.2018.2859582.
[16] J. Liu, A. Vosoogh, A. U. Zaman, and J. Yang, "A slot array antenna with single-layered corporate-feed based on ridge gap waveguide in the 60 GHz band," *IEEE Trans. Antennas Propagat.*, vol. 67, no. 3, pp. 1650–1658, Mar. 2019, doi: 10.1109/TAP.2018.2888730.
[17] M. Akbari, A. Farahbakhsh, and A.-R. Sebak, "Ridge Gap waveguide multilevel sequential feeding network for high-gain circularly polarized array antenna," *IEEE Trans. Antennas Propagat.*, vol. 67, no. 1, pp. 251–259, Jan. 2019, doi: 10.1109/TAP.2018.2878281.
[18] H. Zhao et al., "E-band full corporate-feed 32 × 32 slot array antenna with simplified assembly," *Antennas Wirel. Propag. Lett.*, vol. 20, no. 4, pp. 518–522, Apr. 2021, doi: 10.1109/LAWP.2021.3055763.
[19] W. Lin and R. W. Ziolkowski, "Ka-band huygens antenna array with very high aperture efficiency and low sidelobes," *IEEE Trans. Antennas Propagat.*, vol. 71, no. 1 pp. 1111– 1116, Jan. 2023, doi: 10.1109/TAP.2022.3217179.
[20] M. M. Zhou and Y. J. Cheng, "D-band high-gain circular-polarized plate array antenna," *IEEE Trans. Antennas Propag.*, vol. 66, no. 3, pp. 1280–1287, Mar. 2018, doi: 10.1109/TAP.2018.2796299.
[21] D. Kim, J. Hirokawa, M. Ando, J. Takeuchi, and A. Hirata, "64 x 64-Element and 32 x 32-element slot array antennas using double-layer hollow-waveguide corporate-feed in the 120 GHz band," *IEEE Trans. Antennas Propagat.*, vol. 62, no. 3, pp. 1507–15012, Mar. 2014, doi: 10.1109/TAP.2013.2296318.
[22] Y. Miura, J. Hirokawa, M. Ando, Y. Shibuya, and G. Yoshida, "Double-layer full-corporate-feed hollow-waveguide slot array antenna in the 60-GHz band," *IEEE Trans. Antennas Propag.*, vol. 59, no. 8, pp. 2844–2851, Aug. 2011, doi: 10.1109/TAP.2011.2158784.
[23] J. Hirokawa, T. Tomura, M. Zhang, and M. Ando, "Plate-laminated waveguide slot array antennas for wideband and high-gain operations," in *Proc. 2014 XXXIth URSI General Assembly Scientific Symp. (URSI GASS)*, Beijing, China, Aug. 2014, pp. 1–1. doi: 10.1109/URSIGASS.2014.6929135.
[24] T. Tomura, Y. Miura, M. Zhang, J. Hirokawa, and M. Ando, "A 45° linearly polarized hollow-waveguide corporate-feed slot array antenna in the 60-GHz band," *IEEE Trans. Antennas Propagat.*, vol. 60, no. 8, pp. 3640–3646, Aug. 2012, doi: 10.1109/TAP.2012.2201094.
[25] W. Yuan, X. Liang, L. Zhang, J. Geng, W. Zhu, and R. Jin, "rectangular grating waveguide slot array antenna for SATCOM applications," *IEEE Trans. Antennas Propagat.*, vol. 67, no. 6, pp. 3869–3880, Jun. 2019, doi: 10.1109/TAP.2019.2905784.
[26] T. Li, H. Meng, and W. Dou, "Design and implementation of dual-frequency dual-polarization slotted waveguide antenna array for Ka-band application," *Antennas Wirel. Propag. Lett.*, vol. 13, pp. 1317–1320, 2014, doi: 10.1109/LAWP.2014.2337355.
[27] S. R. Zahran, L. Boccia, G. Amendola, S. Moscato, M. Oldoni, and D. Tresoldi, "Broadband D-band antenna array based on 64 stepped horns for 5G backhauling applications," in *Proc. 2021 15th Eur. Conf. Antennas Propag. (EuCAP)*, Dusseldorf, Germany, Mar. 2021, pp. 1–5, doi: 10.23919/EuCAP51087.2021.9411176.
[28] *Ansys HFSS*, Ansys, Canonsburg, PA, USA, 2018.
[29] T. Zhang, R. Tang, L. Chen, S. Yang, X. Liu, and J. Yang, "Ultra-wideband full-metal planar array antenna with a combination of ridge Gap waveguide and E-Plane groove gap waveguide," *IEEE Trans. Antennas Propagat.*, vol. 70, no. 9, pp. 8051–8058, Sep. 2022, doi: 10.1109/TAP.2022.3165655.
[30] G.-L. Huang, S. Zhou, T.-H. Chio, and T. S. Yeo, "Design of a symmetric rectangular waveguide T-junction with in-phase and unequal power split characteristics," in *Proc. 2013 IEEE Antennas Propagat. Soc. Int. Symp. (APSURSI)*, 2013, pp. 2119–2120, doi: 10.1109/APS.2013.6711718.
[31] S. R. Zahran et al., "Flippable and hermetic *E*-band RWG to GCPW transition with substrate embedded backshort," *IEEE Trans. Microwave Theory Techn.*, vol. 71, no. 6, pp. 2582–2593, Jun. 2023, doi: 0.1109/TMTT.2022.3228619.

SHERIF R. ZAHRAN (Member, IEEE) was born in Cairo, Egypt, in 1991. He received the B.Sc. and M.Sc. degrees from the Arab Academy for Science and Technology, Egypt, in 2013 and 2017, respectively, and the Ph.D. degree from the University of Calabria, Italy, in 2022. He was with Huawei starting from 2015 till 2018 and with Ericsson till 2019 as a Wireless Configuration Engineer. He was a visiting student with the University of Grenoble Alpes, France, and SIAE Microelettronica, Italy. He has more than four years of experience with flexible/wearable wideband monopole antennas and SAR calculations. He has been publishing more than 20 publications in the field of microwave since 2014. His current focus is on developing high gain wideband antenna arrays, transitional structures between circuitry and front-end antennas, and on-chip passive components for millimeter-wave communication applications. He has been a Reviewer for IEEE TRANSACTIONS ON ANTENNAS AND PROPAGATION and *IET Electronics Letters*.

EMILIO ARNIERI (Member, IEEE) was born in Cosenza, Italy, in 1977. He received the degree (Hons.) in information technology engineering from the University of Calabria, Rende, Italy, in 2003, and the Ph.D. degree in electronics engineering from the University Mediterranea of Reggio Calabria, Reggio Calabria, Italy, in 2007. He is currently an Assistant Professor with the Department of Informatics, Modeling, Electronics and System Engineering, University of Calabria, where he has participated in several National, EU, and ESA Projects. He has coauthored more than 80 articles published in international journals and proceedings of international conferences. His current research interests include circular polarizers, the development of dual-band antennas and millimeter-wave components, synthetic aperture radar, and beam scanning antennas. He was selected as a finalist for the Best Paper Award in Antenna Design at the 13th European Conference on Antennas and Propagation in 2019. He serves as an Associate Editor for the IEEE ANTENNAS AND WIRELESS PROPAGATION LETTERS, an Advisory Editor for the *Engineering Reports* (Wiley), and a Guest Editor for *Sensors* (MDPI) and *Electronics* (MDPI). He is the Co-Founder of the academic Spin-off "Antecnica."

STEFANO MOSCATO was born in Pavia, Italy, in 1988. He received the Ph.D. degree in electronics engineering from the University of Pavia, Italy, in 2016. He was a visiting Ph.D. student with Georgia Tech, Atlanta, GA, USA, in early 2015. He became a part of the Research and Development Microwave, SIAE Microelettronica in May 2017. Since September 2022, he has been the Head of the 1337 Research and Development Group devoted to the design and validation of mm-wave passive components, antennas, and subsystems. He is involved in innovation programs and founded researches for microwave backhauling, O-RAN equipment, and space-oriented assemblies. He has authored more than 40 papers on international journals and conferences. His research activities have been focused on RF-to-mm-wave passive component. He was a recipient of an IEEE MTTS Undergraduate/Pre-Graduate Scholarship in 2012. He has been the Chair of the IEEE Student Branch, University of Pavia, since 2013 to 2016.

MATTEO OLDONI (Member, IEEE) was born in Milan, Italy, in 1984. He received the Ph.D. degree in Information Technology from the Politecnico di Milano, Milan, in 2013. He has worked as a Microwave Designer with the Passive Microwave Components Laboratory, SIAE Microelettronica, Milan, where he became a member of Technical Staff, and cooperated with several companies and research institutions internationally. Since June 2022, he has been a full-time Assistant Professor with the Electronics, Information and Bioengineering Department, Politecnico di Milano. His research interests include synthesis and design techniques for microwave filters, algorithms development for computer-aided tuning, and antenna design. He was the recipient of the Young Engineers Prize of the 39th European Microwave Conference.

DARIO TRESOLDI was born in Milan, Italy, in 1955. He received the M.Sc. degree in telecommunications engineering from the Politecnico di Milano, Milan, in 1983. He is currently with SIAE Microelettronica in the field of microwave components. He is involved in the design and developing of microwave filters, couplers, circulators, isolators, and orthomode transducers. He is currently the Supervisor of SIAE Microelettronica Passive Microwave Laboratory.

GIANDOMENICO AMENDOLA (Senior Member, IEEE) received the degree in electrical engineering from the University of Calabria, Rende, Italy, in 1987. From 1988 to 1992, he was a Research Fellow with the Proton Synchrotron Division, European Center for Nuclear Research, Geneva, Switzerland. He is currently an Associate Professor with the Department of Informatics, Modeling, Electronics and System Engineering, University of Calabria, where he is the Director of the Millimeter-wave Antennas and Integrated Circuits Laboratory. His current research interests include antennas, phased arrays, and microwave and millimeter-wave circuits. He was responsible for numerous research projects funded by the European Union and the European Space Agency. He was an Associate Editor of IEEE TRANSACTIONS ON ANTENNAS AND PROPAGATION.

LUIGI BOCCIA (Senior Member, IEEE) was born in Lungro, Italy, in 1975. He received the degree in information technology engineering from the University of Calabria, Rende, Italy, in 2000, and the Ph.D. degree in electronics engineering from the University Mediterranea of Reggio Calabria, Reggio Calabria, Italy, in 2003. From 2005 to 2021, he was an Assistant Professor of Electromagnetics with the University of Calabria, where he is currently an Associate Professor. He is the Co-Editor of the *Space Antenna Handbook* (Wiley, 2012). His current research interests include active antennas, reflectarrays, beam-scanning antennas, and micro- and millimeter-wave IC design. He serves as an Associate Editor for the IEEE MICROWAVE AND WIRELESS COMPONENTS LETTERS, IEEE ANTENNAS AND WIRELESS PROPAGATION LETTERS, and the *International Journal of Microwave and Wireless Technologies* (Cambridge University Press). He is also a member of the European Microwave Association and the Societá Italiana di Elettromagnetismo.

Open Access funding provided by 'Università della Calabria' within the CRUI CARE Agreement